Anhydrous Polyproline Helices and Globules

Anne E. Counterman[†] and David E. Clemmer*

Department of Chemistry, Indiana University, Bloomington, Indiana 47405

Received: August 18, 2003; In Final Form: January 22, 2004

Ion mobility/time-of-flight methods and molecular modeling calculations have been used to examine the conformations of a range of polymer lengths and charge states of polyproline peptides, $[Pro_n + zH]^{z+}$ ($n = 3-56$; $z = 1-6$). Ions formed from 1-propanol solutions {$[Pro_n + H]^+$ ($n = 5-11$) and $[Pro_n + 2H]^{2+}$ ($n = 10-22$)} favor extended forms of the classical polyproline I helix. In these conformers, all proline residues are in the cis configuration, and protonation at the N-terminus allows hydrogen bonds to be formed with backbone carbonyl groups of the second and third proline residues in each polymer. Protonation of this all-cis form at the N-terminus also stabilizes the helix macrodipole. Singly charged ions formed from aqueous solutions favor globular and hairpin-like conformers that contain both *cis*- and *trans*-proline residues. Higher charge state ions ($z = 3-6$) formed from aqueous solutions favor relatively extended conformations, although these are not as extended as the polyproline II structural limit. As polymer size increases, higher charge state ions become more compact. Several conformer states of varying size that appear to be favored structural types are observed; however, we have not been able to identify the type of structures based on comparison of molecular modeling data and experimental measurements.

Introduction

Historically, polyamino acids have served as important model systems in understanding the formation of helical structures.[1] Polyproline is a unique system. The side chain of proline is covalently bound in two sites along the peptide backbone, and the rigidity of the peptide bond gives rise to cis- and trans-residue conformations. In solution and the solid state, polyproline peptides have been shown to exist predominantly in two helical forms: polyproline I (PPI) and polyproline II (PPII), which are shown in Figure 1.[2] PPI is a right-handed helix in which all Pro residues adopt cis configurations; PPII is an extended left-handed helix with all residues in the trans form. These helical forms are unusual in that neither involves stabilization by hydrogen-bonding between backbone −NH and −C═O groups. Extensive experimental work shows that the PPI conformation, which allows van der Waals stabilizing forces to be maximized, exists in nonpolar solutions (such as propanol); PPII (all trans) is found in aqueous solutions.[3,4] The stability of PPII in aqueous solution can be attributed to the formation of hydrogen-bonded networks of water molecules that bridge backbone carbonyl groups of adjacent proline residues; computational and experimental studies have demonstrated the importance of hydration in proline-rich collagen helices (which also adopt a PPII conformation).[5,6] A number of studies have investigated the mutarotation transition between polyproline I and II forms.[7]

Here, we report ion mobility/time-of-flight measurements and molecular modeling studies that are aimed at understanding the gas-phase conformations of polyproline. Several series of polyproline ions, $[Pro_n + zH]^{z+}$ ($n = 3-56$; $z = 1-6$), can be formed by electrospraying[8] aqueous and 1-propanol solutions. Only $[M + H]^+$ and $[M + 2H]^{2+}$ ions are formed from electrospraying 1-propanol solutions. Molecular dynamics simulations of $[Pro_n + H]^+$ ($n = 6$, 8, and 10) suggest that the ions formed from 1-propanol solutions exist as PPI helices that are stretched to accommodate hydrogen-bonding interactions between the N-terminus and two backbone carbonyl groups. Results for $[Pro_n + H]^+$ peptides ($n = 3-11$) generated from aqueous solutions indicate that these ions favor conformers having a distribution of cis and trans forms of proline along the polymer. The mixture of cis and trans residues allows the peptide to adopt relatively compact structures in which the protonated amino terminus is solvated by backbone carbonyl groups. The $[Pro_n + zH]^{z+}$ ions that we observe formed from aqueous solutions are substantially more compact than would be expected if polyproline II forms were retained in vacuo. This result is consistent with earlier solution work reporting that the PPII helix is stabilized by interactions with the solvent. An interesting aspect of these data is that several discrete conformer families are found over the range of polymer lengths and charge states that are observed. Within each charge state, the presence of reproducible peak maxima suggests that polyproline ions of increasing polymer length may fold in a stepwise fashion through favored conformer types, each having a smaller collision cross section.

The structures of proline-containing peptides are also of interest in mass spectrometry studies of biomolecules. Facile cleavage of the peptide bond on the N-terminal side of proline residues has been reported by many groups.[9−12] Work by Breci et al. outlined a relative fragmentation efficiency scale for the Xxx−Pro bond; cleavage of the Pro−Pro and Gly−Pro bonds were found to be the lowest on this scale.[13] We have recently demonstrated that tryptic digest peptides (as well as other small peptides) typically exhibit multiple peaks in ion mobility distributions according to the number of proline residues present.[14] Comparison of experiment with results from molecular modeling studies of the small $[GPGG + H]^+$ system were used to confirm that the peaks we observe arise from the presence

* Corresponding author.
[†] Current address: Department of Chemistry, Pennsylvania State University, University Park, PA 16802.

10.1021/jp036454a CCC: $27.50
Published on Web 03/20/2004

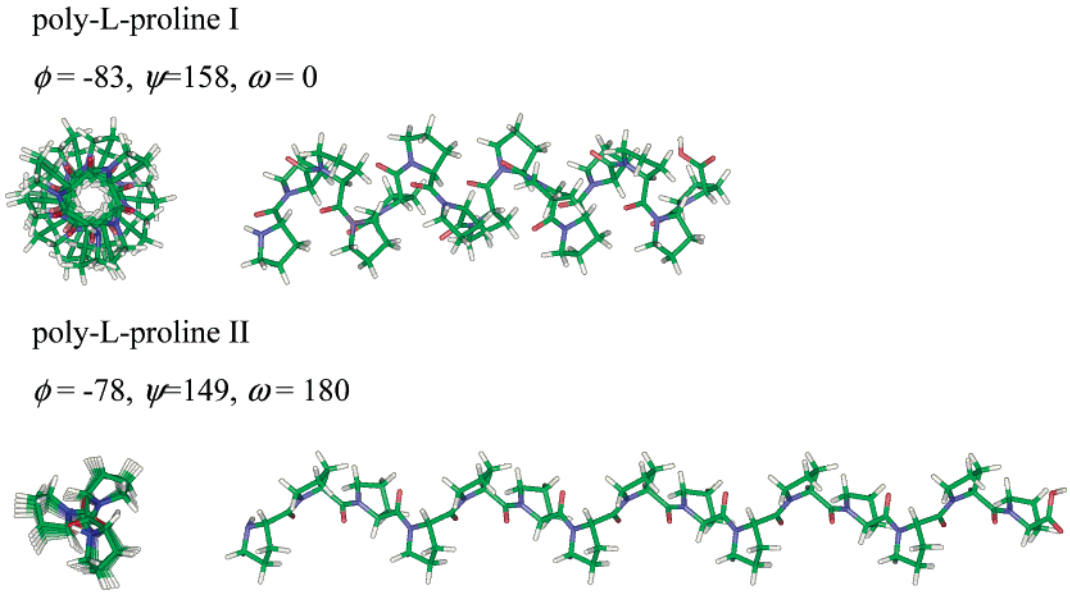

Figure 1. Representation of structures for a 15-residue poly-L-proline. The PPI helix ($\phi = -83°$, $\psi = 158°$, and $\omega = 0°$) contains all cis-residue forms; PPII ($\phi = -78°$, $\psi = 149°$, and $\omega = 180°$) contains all trans-residue forms. Torsion angles are taken from ref 2. Two views of each structure are shown for clarity.

of cis and trans conformations of the Pro residue. More detailed studies of the structures of Pro-containing peptides may lead to a better understanding of the fragmentation work.

A number of recent gas-phase studies have focused on the stability of α-helical motifs in small (10−20 residue) alanine-rich peptides.[15−21] Recent studies by Jarrold and co-workers have demonstrated that $[Ac\text{-}Leu_n + H]^+$ ($n = 5-19$) form exceptionally stable α-helices in vacuo.[22] Other studies in which a block of Gly residues were placed in the center of an alanine-based polymer demonstrate that a large fraction of Gly residues is required to disrupt helix formation.[17,19] We recently presented evidence that $[Ala_n + 3H]^{3+}$ peptides ($n = 18-41$) form two conformer states in the gas phase: a folded state that we assign to a hinged helix-coil, and an extended helical state.[20] In these studies,[20] as well as in studies of singly protonated alanine-based polymers,[15] placing the net location of charge toward the C-terminal end of the polymer stabilizes the helix macrodipole. Additionally, we have assessed the fraction of $i \rightarrow i + 4$ and $i \rightarrow i + 3$ hydrogen-bonding interactions in alanine helices, $[Ala_n + 4H]^{4+}$, where $n = 29-49$.[23] The relative populations of the hinged helix-coil, α-, and 3_{10}-helices are highly dependent upon protonation state, proton location, and polymer size. The studies presented here are the first to delineate the solution dependence of helical polyproline conformers in the gas phase.

Experimental Section

Ion Mobility/Time-of-Flight Methods. Experiments were performed using an ion mobility/time-of-flight instrument that has been described in detail previously.[24,25] This instrument utilizes a high-pressure source, and mobilities (cross sections) are measured before ions are extracted into a vacuum region; thus, ion conformations are established under very gentle ionization conditions which are often influenced by the solvent composition used.[26,27] Solutions of a mixture of poly-L-proline sizes (Sigma, 1000−10 000 mol wt; ~5×10^{-5} to 5×10^{-4} M in 49:49:2 water/methanol/acetic acid or 99.8:0.2 1-propanol/HCl) were electrosprayed[8] into a differentially pumped desolvation region and introduced into a helium-filled drift region. Separate experiments were performed in which polyproline solutions (at the same concentrations as given above) were nanosprayed from completely aqueous solutions, and the results are similar to those reported for the water/methanol/acetic acid solvent system. Thus, we refer to the water/methanol/acetic acid solution as *aqueous*.

Ion mobility and mass-to-charge ratio measurements for mixtures of ions are obtained by a nested drift (flight) time acquisition scheme.[24] The mobilities of the polypeptide ions through the gas under the influence of a weak uniform electric field (137.4 V·cm^{-1}) depend on the polypeptide shapes[28,29] and charge states.[30,31] For a given charge state, compact geometries with relatively small collision cross sections have higher mobilities than more elongated structures.[28,32,33] Ions experience drift forces that are proportional to their charge states (and the applied drift field). Flight times were measured in a reflectron geometry time-of-flight mass spectrometer and are much shorter than drift times, allowing the mixture of ions to be analyzed in a nested fashion.[24]

Experimental Collision Cross Sections. The measured arrival times include the time required for ions to travel through drift gas as well as other regions of the instrument. To determine cross sections, it is necessary to obtain the drift times (the time ions spend drifting through the drift region). These values are obtained by correcting the arrival times by the time ions spend in other regions of the instrument. These corrections are small (80−140 s) relative to the 10−30 ms drift times. Experimental collision cross sections are derived from the corrected arrival times by the following relation[34]

$$\Omega = \frac{(18\pi)^{1/2}}{16}\frac{ze}{(k_B T)^{1/2}}\left[\frac{1}{m_I}+\frac{1}{m_B}\right]^{1/2}\frac{t_D E}{L}\frac{760}{P}\frac{T}{273.2}\frac{1}{N} \quad (1)$$

where t_D is the drift time (determined from the maximum of each peak), E is the drift field; T and P are the temperature and pressure of the buffer gas, respectively; L is the drift tube length; ze, the ion's charge; N, the neutral number density; k_B, Boltzmann's constant; and m_I and m_B, the masses of the ion and buffer gas, respectively. The parameters E, L, P, T, and t_D can be precisely measured. The reproducibility of measured cross sections is high; the percent relative uncertainty of any two measurements is typically less than ±0.5%. Measurements

were performed at low *E*/*N* such that mobilities are independent of the applied drift field and drift velocities are small compared with the thermal velocity of the buffer gas. Under these conditions, ions are not expected to align in the drift tube and we assume that collision cross sections correspond to an average of all possible orientations.

An Effective Asphericity Scale. Collision cross sections show a strong correlation with molecular weight; because of this, it is useful to plot cross section values on a modified scale that removes the molecular weight dependence. For this purpose, we have previously described an *effective asphericity* scale (Ω_{asp}).[19] *Effective asphericities* for different peptide lengths (*n*) are determined from experimental or calculated cross sections (Ω) using

$$\Omega_{asp} = \frac{\Omega - \Omega_{sphere}}{\Omega_{linear} - \Omega_{sphere}} \quad (2)$$

where Ω_{sphere} and Ω_{linear} are cross sections calculated from fits to globular and extended linear geometries of the model polyalanine system, as described previously.[35] On this scale, Ω_{asp} for compact globular ions is defined to be 0.0 (determined by a fit to experimental values for $[Ala_n + H]^+$ ions having roughly spherical, tightly packed globular conformations in which the protonated amino terminus is solvated by electronegative carbonyl groups along the polymer backbone). Values of Ω_{asp} for completely extended linear Ala_n polymers are defined to be 1.0.

Molecular Modeling Simulations and Calculation of Cross Section for Model Geometries. More details about the conformations adopted by polyproline ions can be obtained from molecular modeling simulations. We performed simulations for the following charge states and sizes: $[Pro_n + H]^+$ $n = 6$, 8, and 10; $[Pro_n + 2H]^{2+}$ $n = 10$, 15, and 20; and $[Pro_n + 3H]^{3+}$ $n = 15$ and 25. Molecular dynamics simulations were carried out at 300 K for at least 0.25 ns (and in some cases, up to 1.0 ns) using the extensible systematic force field (ESFF) and a dielectric of 1.0. This approach is analogous to the methods we have used previously[19] and similar to approaches taken by others.[15,22] Simulations of each $[Pro_n + H]^+$ polymer size assumed that a proton was located at the N-terminus; this is expected to be the most basic site.[36] As demonstrated previously for the polyalanine system, the location of protons has a strong influence on peptide geometry.[19] For the $[Pro_n + 2H]^{2+}$ and $[Pro_n + 3H]^{3+}$ ions, many proton configurations are possible. At least eight proton configurations were chosen for each polymer size. Widely different proton configurations were chosen to gain insight into the effects of proton placement on overall polymer geometry. All protons were assumed to be located on the nitrogen of backbone imide groups.[37] We denote proton locations according to the residue number of the protonated imide group; that is, for a doubly protonated ion, protonation at the N-terminus and the imide of the fifth residue would be referred to as a (1,5) configuration. Similarly, charge site configurations for triply protonated ions are given as ordered triplets [e.g., (1,8,15)]. Another critical consideration for the polyproline system is the starting geometry used for simulations. A particular concern is the ability to sample both cis and trans configurations of proline residues over the time scale of the simulations. Experimental studies in solution have measured a barrier of ~19 to 20 kcal·mol^{-1} for the cis to trans interconversion;[38,39,40] simulations of dipeptides indicate that the barrier to interconversion in the gas phase is slightly lower, ~15.7 kcal·mol^{-1}.[41] Simulations were started from both PPI (all cis) and PPII (all trans) helical forms as well as from several geometries in which the number and location of *cis*- and *trans*-proline residues were randomized. More details about which residues were randomized over cis and trans forms for specific charge states and polymer sizes are given below. Overall, the variability in charge assignment position as well as cis- and trans-residue location makes this a very complicated system to sample with molecular mechanics simulations. The starting structures that we have used clearly do not assess all possible configurations, but do provide an initial look at some possible structural types.

Calculation of Cross Sections for Trial Conformers Generated by Molecular Modeling. Cross sections for trial conformers were calculated using the exact hard spheres scattering method (EHSS),[42] and the resulting values were normalized using a calibration obtained from comparison of values calculated for hundreds of peptides using EHSS and the more rigorous, but computationally expensive, trajectory method.[43] Agreement between calculated values and experimentally measured collision cross sections was required to be within 2% in order for a geometry to be considered as a viable representation. In some cases, a direct comparison of values calculated for trial geometries with experimental drift time distributions is instructive. Drift times can be derived from calculated cross sections using the experimental parameters and eq 1.

Results and Discussion

Ion Mobility/Time-of-Flight Data for Ions Formed by Electrospraying Aqueous and Propanol Solutions. Figure 2a shows a two-dimensional plot of a small range (m/z = 580−760) of data recorded by electrospraying polyproline from a water/methanol mixture. Over this range, ions representing six charge states are assigned. For example, the peaks at m/z ratios of 601.5, 641.0, 719.1, 612.4, 645.4, and 602.9 are assigned to $[Pro_6 + H]^+$ (which has a calculated m/z_{calc} value of 601.6),[44] $[Pro_{13} + 2H]^{2+}$ (m/z_{calc} = 641.2), $[Pro_{22} + 3H]^{3+}$ (m/z_{calc} = 719.1), $[Pro_{25} + 4H]^{4+}$ (m/z_{calc} = 612.4), $[Pro_{33} + 5H]^{5+}$ (m/z_{calc} = 645.5), and $[Pro_{37} + 6H]^{6+}$ (m/z_{calc} = 602.8), respectively. Over the entire data set, we assign $[Pro_n + H]^+$, $n = 3-10$; $[Pro_n + 2H]^{2+}$, $n = 9-20$; $[Pro_n + 3H]^{3+}$, $n = 14-29$; $[Pro_n + 4H]^{4+}$, $n = 19-43$; $[Pro_n + 5H]^{5+}$, $n = 23-47$; and $[Pro_n + 6H]^{6+}$, $n = 31-56$. The $[Pro_n + 2H]^{2+}$ ions have much higher mobilities (appearing at shorter drift times) than $[Pro_n + H]^+$ ions of comparable m/z ratios. However, mobilities for many of the $[Pro_n + 2H]^{2+}$ and $[Pro_n + 3H]^{3+}$ ions of comparable m/z ratios are similar. Additionally, for m/z values above ~700, the mobilities of $[Pro_n + H]^+$, $[Pro_n + 4H]^{4+}$, $[Pro_n + 5H]^{5+}$, $[Pro_n + 6H]^{6+}$ ions are such that many peaks begin to converge along a single line in the two-dimensional data set.

Figure 2b shows a two-dimensional plot for polyproline ions formed from a 1-propanol solution (and otherwise recorded under similar experimental conditions to the data shown in Figure 2a). Only $[Pro_n + H]^+$ and $[Pro_n + 2H]^{2+}$ ions are apparent in this data set; no contributions from higher charge states ($z \geq 3$) are found. The mobilities of the $[Pro_6 + H]^+$ ion formed from aqueous and propanol solutions are essentially identical. However, the $[Pro_n + H]^+$ ($n = 7-11$) and $[Pro_n + 2H]^{2+}$ ($n = 12-15$) ions observed in the data set recorded for propanol solution appear at longer drift times than their counterparts formed from aqueous solution. A summary of the drift times and cross sections for relatively small polymer sizes that are observed upon electrospraying the aqueous and propanol solutions is given in Table 1.

Another comparison of the two data sets can be obtained by comparing drift time distributions (derived by integrating the

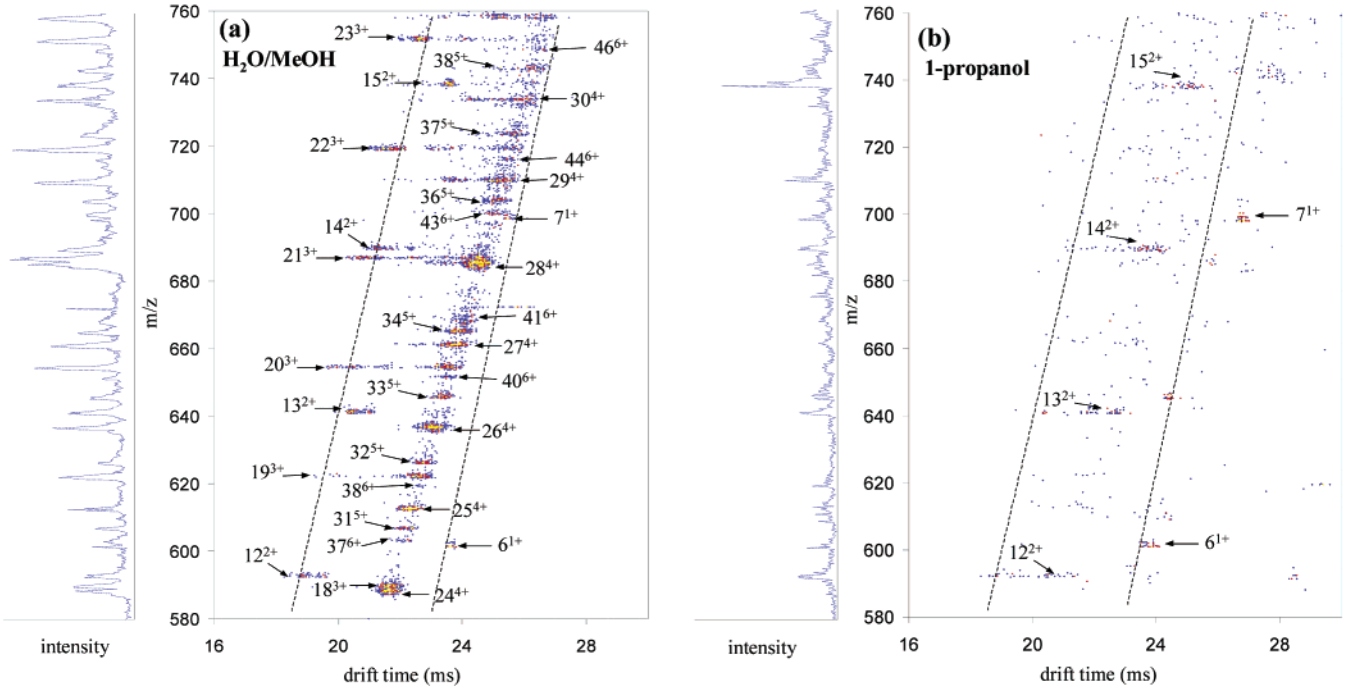

Figure 2. A representative region of data recorded for polyproline mixtures electrosprayed from (a) 49:49:2 water/methanol/acetic acid solution and (b) 99.8:0.2 1-propanol/HCl solution. The dashed lines are intended only as a visual guide to the general locations of the $[M + H]^+$ and $[M + 2H]^{2+}$ peaks observed by electrospraying from the aqueous-based solution. The data sets are normalized to a buffer gas pressure of 150.00 Torr and an electric field strength of 137.4 V·cm^{-1}. For each data set, the mass spectrum on the left shows the integrated intensities for each *m*/*z* window.

two-dimensional data over a range of flight times that corresponds to a single *m*/*z* ratio). Figure 3 shows distributions for $[Pro_n + H]^+$ ions ($n = 6-8$) formed from each solution type. In all of the distributions except $[Pro_9 + H]^+$, the distribution is dominated by a single, sharp peak. The $[Pro_8 + H]^+$ distribution (aqueous) shows a second, smaller feature at longer times (~29 ms). Drift times for the major peak observed in each $[Pro_n + H]^+$ (propanol) distribution are higher than those for their $[Pro_n + H]^+$ (aqueous) counterparts (Table 1). For $[Pro_5 + H]^+$, the difference is small [20.82 ms (aqueous) and 21.18 ms (propanol)]. By $[Pro_{10} + H]^+$, the difference is substantial: a difference of >3 ms is observed between the aqueous and propanol distributions.

Figure 4 shows drift time distributions for $[Pro_n + 2H]^{2+}$ (aqueous and propanol). Each mobility distribution shows that peaks are substantially broader than those observed for the $[Pro_n + H]^+$ ions and fall over a range of drift times. This indicates that a range of conformer sizes are present; we note that both differences in protonation patterns and the presence of many low-energy or kinetically trapped conformers for each specific proton configuration may be responsible for the increased peak width of the $[Pro_n + 2H]^{2+}$ distributions. In general, the $[Pro_n + 2H]^{2+}$ distributions observed from propanol solution are narrower than those of the corresponding ions formed from aqueous solutions. Multiple resolved features are present in many of the distributions (in particular, the $[Pro_{14} + 2H]^{2+}$ and $[Pro_{18} + 2H]^{2+}$ distributions obtained from aqueous solution). The distributions observed from aqueous solution each contain broad features ~5 ms in width that are found underlying each dominant peak. The $[Pro_{14} + 2H]^{2+}$ (aqueous) distribution contains large, well-separated features (at ~21.0, 22.3, and 24.5 ms). By $[Pro_{16} + 2H]^{2+}$, one peak appears to dominate the distribution at 24.8 ms. Two large features are resolved in the $[Pro_{18} + 2H]^{2+}$ distribution at 27.2 and 26.6 ms. Drift times recorded for the dominant peak in each distribution are again higher for ions obtained from the propanol solution, with a single exception ($[Pro_{10} + 2H]^{2+}$).

Comparison of data for the $[Pro_n + H]^+$ and $[Pro_n + 2H]^{2+}$ ions where $n = 10$ and 11 (the only polymer sizes observed in both solutions for both $z = 1$ and 2) is also interesting. We note that the drift times for different charge state ions cannot be directly compared without normalization for charge state (e.g., by using a collision cross section scale). The collision cross section for $[Pro_{10} + 2H]^{2+}$ (aqueous) is substantially higher than that of $[Pro_{10} + H]^+$ (aqueous); however, addition of a single proton in the propanol system leads to only a slight increase in collision cross section (2.4%). A similar observation is made for $[Pro_{11} + H]^+$ and $[Pro_{11} + 2H]^{2+}$, as well as for the nine-residue polymer (only observed as a doubly protonated ion in the aqueous solution). Clearly, addition of a proton has a substantial impact on the structure of the ions formed from aqueous solution. Conversely, the similarity of collision cross sections for the $[Pro_n + H]^+$ and $[Pro_n + 2H]^{2+}$ ions (propanol; $n = 10$ and 11) suggests that the structures of these ions may be similar.

Collision Cross Sections for $[Pro_n + zH]^{z+}$ Ions Formed by Electrospraying Aqueous Solutions. As demonstrated above, the raw data (and slices through these data to obtain mobility distributions) show that electrospraying aqueous solutions leads to a very complex system. That is, we observe a range of polymer lengths and charge states, and within these, multiple conformations exist. Information about the general trends that are present in these data can be obtained by examining Figure 5. This figure shows collision cross sections (determined from measured drift times using eq 1) for the reproducible peak maxima found by electrospraying the aqueous solutions. Additionally, the vertical lines show the range of features that are observed for specific sizes and charge states.

Overall, the cross sections of polyproline peptides increase with increasing size. Small polymer lengths (~3 to 10 residues)

TABLE 1: Summary of Drift Times and Collision Cross Sections for Large Peaks Observed for Small $[Pro_n + H]^+$ and $[Pro_n + 2H]^{2+}$ Ions Formed by Electrospraying Aqueous and Propanol Solutions

	aqueous		propanol		model geometries		
n	t_D (ms)[a]	Ω_{expt} (Å^2)[b]	t_D (ms)	Ω_{expt} (Å^2)	initial geometries[c]	figure[d]	Ω_{calc} (Å^2)[e]
				$[Pro_n + H]^+$			
3	15.04	104.8					
4	18.27	127.4					
5	20.82	145.2	21.18	147.8			
6	23.71	165.5	24.05	167.9	PPI	8a	
					PPII	8b	
7	25.41	177.4	26.94	188.1			
8	27.79	194.0	29.99	209.4	PPI	8a	211.5
					PPII	8b	197.6
9	30.39	212.3	32.80	229.2			
10	32.54	227.4	35.68	249.3	PPI	8a	252.5
					PPII	8b	268.9
					rand	8c (1)	230.6
					rand	8c (2)	228.3
					rand	8c (3)	229.9
11	34.19	238.9	38.68	270.3			
				$[Pro_n + 2H]^{2+}$			
9	17.82	247.8					
10	18.95	263.6	18.35	255.3	PPI (1,2)	9b	227.8
					PPI (1,5)	9a,b	242.5
					PPI (1,10)	9b	245.3
					PPI (5,10)	9b	259.3
11	18.10	251.7	19.70	273.9			
12	18.84	262.0	20.85	290.0			
13	20.42	284.2	22.87	318.3			
14	21.22	295.3	24.37	339.2			
15	23.59	328.7	25.27	352.1	PPI (1,7)	9a	345.0
					PPII (1,2)	9c	297.6
					PPII (1,7)	9c	326.3
					PPII (1,15)	9c	375.4
					PPII (7,15)	9c	340.8
16	24.78	345.4	26.42	368.2			
17	25.92	361.3	27.34	381.1			
18	27.16	378.8	28.72	400.5			
19	29.48	411.4	30.14	420.6			
20	29.60	413.0	31.47	439.2	PPI (1,10)	9a	442.4
21			33.02	459.4			
22			34.31	477.1			

[a] Drift times are normalized to 150.00 Torr and an electric field strength of 137.4 V·cm^{-1}. [b] Experimental collision cross sections were determined from measured drift times using eq 1. [c] The initial geometry from which molecular dynamics simulations were initiated is given as PPI, PPII, or "rand" (which indicates that cis- and trans-residue forms were randomized throughout the polymer). Numbers in parentheses for the $[Pro_n + 2H]^{2+}$ ions indicate the positions of proton placement in the simulation (i.e., 1 denotes protonation of the amino terminus). [d] Denotes the figure in which each model conformer is presented. [e] Collision cross sections for model conformers were calculated as described in the experimental section.

are restricted to a narrow range of different shapes compared with larger polymers (e.g., the different $[Pro_{55} + 6H]^{6+}$ ion structures span a ~300 Å^2 range of cross sections). It is interesting to note that at 50 residues, polyproline ions (having a mass of ~4000 Da) have cross sections that are similar to values we have measured for compact states of the much larger cytochrome *c* protein (~12 kDa).[27,29] This indicates that even the most compact forms of polyproline are not packed to the degree that is observed for protein sequences. Presumably the restrictions imposed on backbone torsion angles by the proline residue prohibit tight packing interactions associated with protein tertiary structure.

Other details of this system are also quite interesting. As observed from the mobility distributions, the data recorded for $z \geq 2$ ions (while exhibiting distinct peaks) typically also show broad underlying features; the ranges of these broad features are indicated by the error bars shown. The peaks appear to fall into families, suggesting that specific types of conformations may be favored within specific ranges of polymer sizes. The most extended conformers within each charge state (for $z \geq 2$) are observed at small polymer sizes (presumably due to higher Coulombic repulsion between charges). As polymer length increases, new ions having smaller collision cross sections are observed. These longer polymer chains may fold. Ion mobility distributions for the $[Pro_n + 3H]^{3+}$ ions exhibit peaks that appear to be related as a function of size. These families are observed over the size ranges $n = 14-21$ (low mobility) and $n = 22-29$ (high mobility). The $[Pro_n + 4H]^{4+}$ ions exhibit three families of conformers that are dominant over the $n = 19-31$ (low mobility), $n = 32-35$, and $n = 36-44$ (high mobility) size ranges. The lowest mobility family of $[Pro_n + 5H]^{5+}$ ions is observed for $n = 25-40$. It appears that there is a critical size for forming the most compact state: $n = 12$, 22, and ~42 for $[Pro_n + 2H]^{2+}$, $[Pro_n + 3H]^{3+}$, and $[Pro_n + 4H]^{4+}$, respectively. At each of these sizes, a structure (or group of related structures) that is the most compact within each charge state becomes favored. Above this size, no additional collapse is observed.

The number of conformer families observed in each charge state (defined by peak maxima) increases with increasing charge state for $z = 1-4$. In the case of $[Pro_n + 5H]^{5+}$ and $[Pro_n + 6H]^{6+}$ ions, distributions are broad and poorly resolved, making it difficult to track peak maxima other than the dominant feature in most cases. The increase in number of conformer families

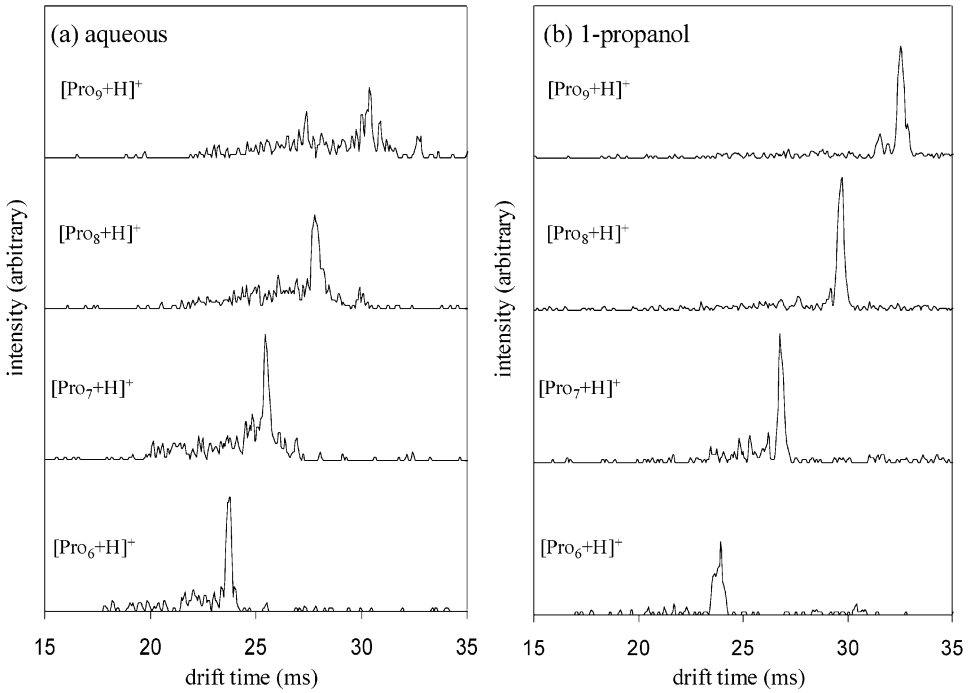

Figure 3. Drift time distributions for $[Pro_n + H]^+$ ions ($n = 6-9$) formed by electrospraying from (a) 49:49:2 water/methanol/acetic acid and (b) 99.8:0.2 1-propanol/HCl solutions. Data are normalized to a buffer gas pressure of 150.00 Torr and an electric field strength of 137.4 V·cm^{-1}.

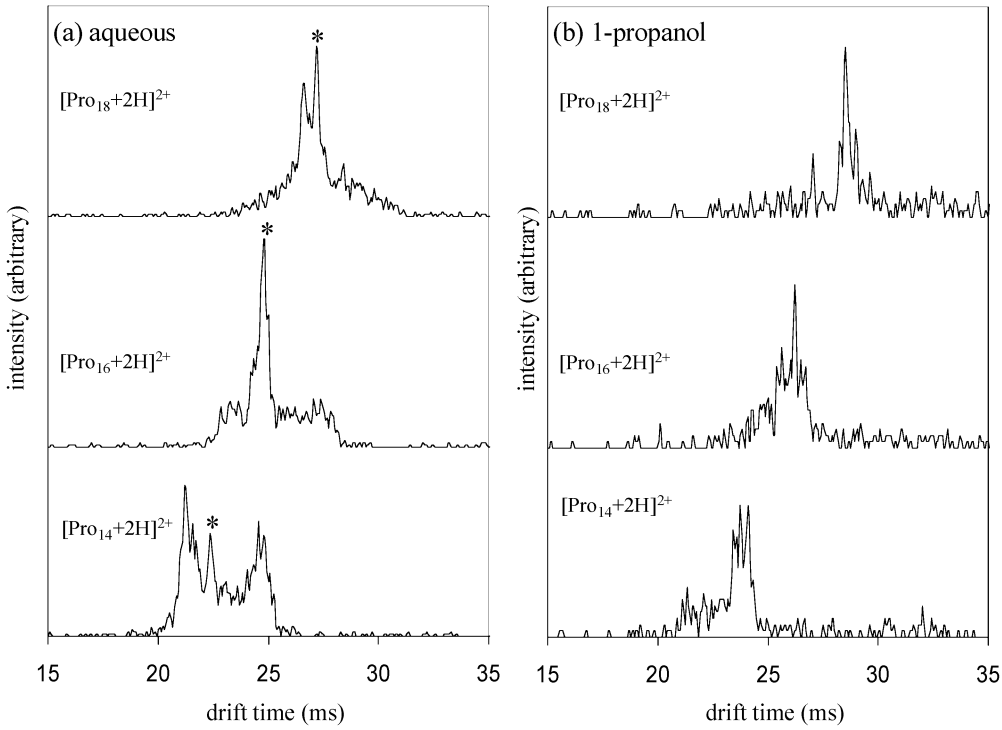

Figure 4. Drift time distributions for $[Pro_n + 2H]^{2+}$ ions ($n = 14$, 16, and 18) formed by electrospraying from (a) 49:49:2 water/methanol/acetic acid and (b) 99.8:0.2 1-propanol/HCl solutions. Data are normalized to a buffer gas pressure of 150.00 Torr and an electric field strength of 137.4 V·cm^{-1}. Asterisks in (a) indicate maxima of a series of peaks (for increasing polymer size) that are identified as a conformer family (see Figure 5 and text).

with charge state may indicate that protonation sites are important in a stepwise rearrangement of the polymer chain.

To provide an example of the behavior observed for high charge states in this system, mobility distributions for $[Pro_n + 3H]^{3+}$ and $[Pro_n + 4H]^{4+}$ ions (aqueous) are shown in Figure 6. Distributions for both charge states are dominated by a single sharp peak at small polymer lengths ($[Pro_{16} + 3H]^{3+}$, $[Pro_{22} + 4H]^{4+}$, and $[Pro_{25} + 4H]^{4+}$). Larger polymer sizes ($[Pro_{19} + 3H]^{3+}$ and $[Pro_{28} + 4H]^{4+}$) show additional features at shorter drift times. At these larger polymer sizes, distributions are very broad (spanning ~4 to 5 ms); however, resolved features are often observed in these broad distributions (e.g., $[Pro_{22} + 3H]^{3+}$). These results are similar to those reported previously for proteins; high charge state protein ions exhibit sharp peaks in the ion mobility distributions.[24] The reduction in Coulombic energy associated with lower charge states allows these ions to

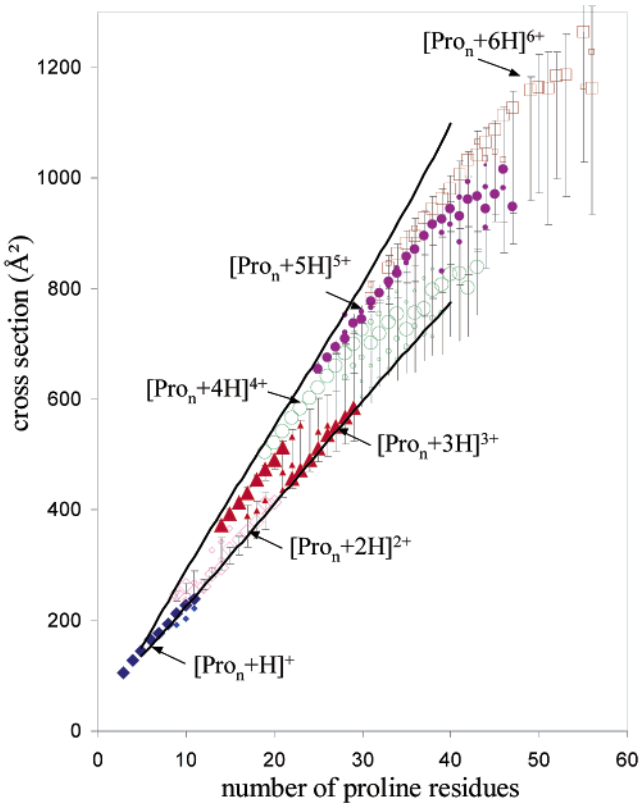

Figure 5. Collision cross sections derived from peak maxima observed for $[Pro_n + zH]^{z+}$ ($n = 3-56$, $z = 1-6$) ions electrosprayed from 49:49:2 water/methanol/acetic acid solutions. Symbols correspond as follows: solid diamonds, $[Pro_n + H]^+$ ions; open diamonds, $[Pro_n + 2H]^{2+}$; solid triangles, $[Pro_n + 3H]^{3+}$; open circles, $[Pro_n + 4H]^{4+}$; solid circles, $[Pro_n + 5H]^{5+}$; open squares, $[Pro_n + 6H]^{6+}$. Larger symbol sizes are used to denote cross sections corresponding to the most intense peak observed for each polymer size and charge state. Error bars represent ranges of collision cross sections observed for broad, poorly resolved peaks.

adopt more compact geometries; mobility distributions for lower charge state protein ions are also typically very broad and indicate that a wide array of different conformer types are present. The sharp peaks for $[Pro_{16} + 3H]^{3+}$ and $[Pro_{22} + 4H]^{4+}$ each correspond to a family of relatively extended conformers (having cross sections shown in Figure 5). The asterisks in Figure 6 show the location of the two conformer families as polymer size increases.

Effective Asphericities for $[Pro_n + zH]^{z+}$. Another useful way to view these data is by plotting cross sections on an *effective asphericity* scale, as described above. Figure 7 shows experimental asphericities for the dominant peak observed in each $[Pro_n + zH]^{z+}$ ($n = 3-56$, $z = 1-6$) from aqueous and propanol solutions. Asphericities for $[Pro_n + H]^+$ ($n = 7-11$) and $[Pro_n + 2H]^{2+}$ ($n = 11-22$) are substantially higher for the ions obtained from propanol solutions than from aqueous solutions. Comparison of the measured $[Pro_n + H]^+$ asphericities with the calculated asphericities for an ideal PPI helix (over a range of polymer sizes) shows that ions obtained upon electrospraying propanol solutions are slightly larger than expected for the ideal PPI helix. The $[Pro_n + H]^+$ ($n = 7-11$) ions (aqueous) are more compact and approach the asphericities measured for $[Ala_n + H]^+$ globules. This comparison suggests that the $[Pro_n + H]^+$ ($n = 7-11$) ions (aqueous) have roughly spherical (globular) structures.

The $[Pro_n + 2H]^{2+}$ (propanol) ions are more aspherical than the calculated values for the ideal PPI helix at small n; however, by n values of 14 and higher, asphericities track the PPI line. This comparison suggests that $[Pro_n + 2H]^{2+}$ (propanol) ions ($n = 14-19$) may indeed adopt PPI helical conformations. Below, we present molecular modeling results that are consistent with this preliminary assignment. This said, $[Pro_n + 2H]^{2+}$ peptides of the same size range formed upon electrospraying aqueous solutions are considerably more compact. Thus, these polyproline ions can also adopt geometries that are more spherical (more compact) in nature.

The dominant conformer families for $[Pro_n + 3H]^{3+}$ ($n = 14-21$), $[Pro_n + 4H]^{4+}$ ($n = 19-30$), and $[Pro_n + 5H]^{5+}$ ($n = 25$ to ~38) have higher asphericities than those calculated for ideal α-helices or measured for the helical $[Ala_nLys + H]^+$ or $[Ala_n + 3H]^{3+}$ ions. Note that these data are compared on a molecular weight scale; thus, for a given molecular weight, the proline polymers contain fewer residues than the alanine polymer. As the number of residues exceeds 22, a new, more compact dominant conformer family emerges for the series of $[Pro_n + 3H]^{3+}$ ions (Figure 5). The most compact conformer families for each charge state (i.e., $[Pro_n + 2H]^{2+}$ $n = 15-20$, $[Pro_n + 3H]^{3+}$ $n = 22-29$, and $[Pro_n + 4H]^{4+}$ $n = 36-44$) appear to fall roughly along a line that is systematically lower than the calculated values for the PPI helix. This suggests that these ions (produced by electrospraying aqueous solutions) may adopt a structures that can propagate with increasing polymer size. Although we have not investigated this rate of change of asphericity with polymer length in detail, the similarity with the PPI form (favored for propanol solutions) leads us to speculate that the PPII (aqueous helix) may collapse into a more compact helix upon removal of the solvent. We are currently carrying out molecular modeling studies in order to consider the idea that other types of more compact (all *trans*-proline) structures may be stable; for example, it is possible that a helical-like structure (more compact than the PPI helix) or a hinged helix-coil motif, as was observed for polyalanine ions, will fit these data.

Molecular Dynamics Simulations of $[Pro_n + H]^+$. In order to begin to understand the differences in conformations of small $[Pro_n + H]^+$ ions formed from different solution conditions, we performed molecular modeling simulations of the $n = 6$, 8, and 10 polymer lengths. Figure 8 shows model conformers for the lowest energy $[Pro_6 + H]^+$, $[Pro_8 + H]^+$, and $[Pro_{10} + H]^+$ geometries obtained from simulations initiated from PPI and PPII helical forms. The conformers obtained using PPI starting structures are lower in energy for all three polymer sizes than geometries obtained from PPII starting structures. The PPI-derived geometries retain a high degree of similarity to the original PPI structure. A key difference between the low-energy protonated geometries and an ideal PPI helix is that (for all three polymer sizes) the protonated N-terminus is oriented such that hydrogen bonds can be formed with carbonyl groups of the second and third residues in the polymer chain. The collision cross sections for the PPI-like model geometries (211.5 and 252.5 Å^2) are close to the 209.4 and 249.3 Å^2 experimental values for $[Pro_8 + H]^+$ and $[Pro_{10} + H]^+$ (propanol), respectively. An important consideration in stabilizing this PPI-like helical form is that the macrodipole of the helix points in the direction of the N-terminus; thus, unlike alanine polymers, protonation at the N-terminus stabilizes an all *cis*-proline helix.

Figure 8c shows geometries obtained from simulations in which the *cis*- and *trans*-proline content was randomized in the starting structures. A number of low-energy geometries were found that are consistent with the experimental collision cross section for $[Pro_n + H]^+$ ($n = 6$, 8, and 10) ions generated from

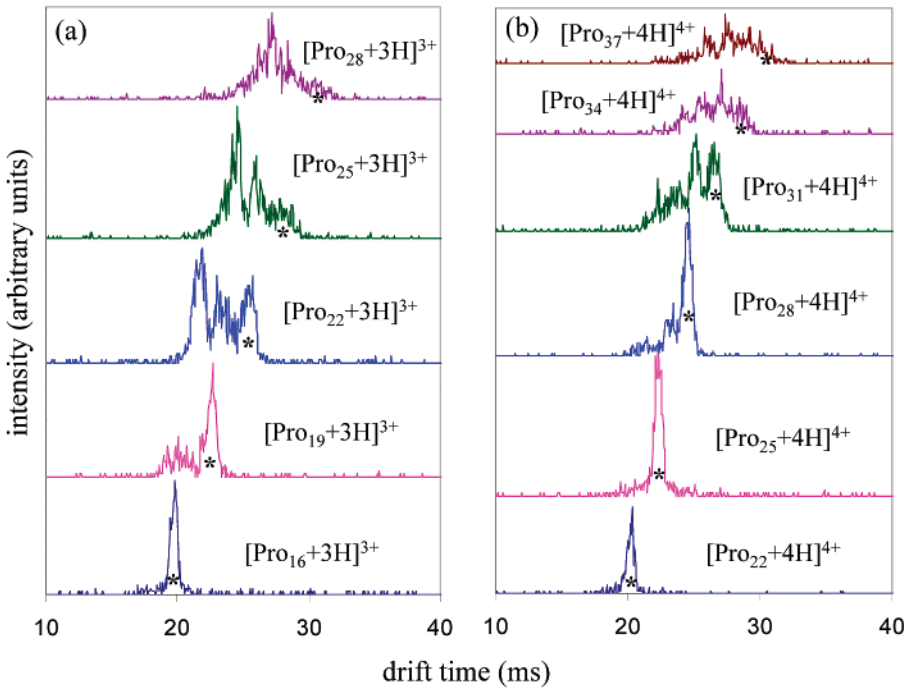

Figure 6. Drift time distributions for $[Pro_n + 3H]^{3+}$ (n = 16, 19, 22, 25, and 28) ions and $[Pro_n + 4H]^{4+}$ (n = 22, 25, 28, 31, 34, and 37) ions formed by electrospraying from 49:49:2 water/methanol/acetic acid solution. Data are normalized to a buffer gas pressure of 150.00 Torr and an electric field strength of 137.4 V·cm^{-1}. Asterisks indicate the location of an extended conformer family in each charge state.

aqueous solution. These conformers adopt relatively compact geometries in which the N-terminal protonation site forms hydrogen-bonding interactions with multiple (~3 to 4) backbone carbonyl groups. The second Pro residue (adjacent to the N-terminal charge site) was typically found in the cis form and the third Pro residue adopted a *trans*-Pro configuration, allowing a hydrogen bond to form between the carbonyl of the second residue and the charge site. No other correlations of position and isomeric form were noted. We conclude that the compact states arise from mixtures of cis- and trans-residue forms along the polymer. The exact positions of cis and trans forms may not be important in defining these structures, as many different cis- and trans-residue combinations appear to be consistent with these data.

Structural Characterization of $[Pro_n + 2H]^{2+}$ (Propanol) Ions. We begin our analysis of $[Pro_n + 2H]^{2+}$ peptides by considering the ions formed from propanol solution. Several charge site configurations were assessed using PPI starting geometries; of the protonation configurations examined in which one of the protons was fixed at the N-terminus [e.g., (1,2), (1,*n*/2), (1,*n*)], the (1,*n*/2) configurations had the lowest energy. Figure 9a shows low-energy conformers obtained for the (1,*n*/2) charge site configuration of $[Pro_{10} + 2H]^{2+}$, $[Pro_{15} + 2H]^{2+}$, and $[Pro_{20} + 2H]^{2+}$. All of these conformers retain the all-cis content of the starting structure and are slightly stretched relative to an ideal PPI structure. Collision cross sections calculated for the $[Pro_{15} + 2H]^{2+}$ and $[Pro_{20} + 2H]^{2+}$ conformers shown are in good agreement with experiment (within 2.0 and 0.7%, respectively). The only geometries (over simulations of PPII and torsion-angle-randomized starting geometries for many charge site assignments) that had lower calculated energies than these stretched PPI geometries were very compact, globular conformations formed by protonating sites near the N-terminus on a PPII geometry; these globules were ruled out because they had cross sections substantially lower than experiment.

We note that the $[Pro_{10} + 2H]^{2+}$ (1,5) conformer shown in Figure 9a has a calculated cross section that is 5% lower than experiment (outside the range that we consider as viable structural representations). Figure 9b shows geometries for other charge site assignments for $[Pro_{10} + 2H]^{2+}$. The geometry that is in closest agreement with experiment is the (5,10) conformer (Ω_{calc} = 259.3; Ω_{expt} = 255.3), in which the helix has unraveled. This demonstrates that at the smallest polymer sizes, the van der Waals stabilization of the PPI-like helix geometry is insufficient to balance the larger Coulombic repulsion experienced in these ions.

Structural Characterization of $[Pro_n + 2H]^{2+}$ (Aqueous) Ions. Mobility distributions for $[Pro_n + 2H]^{2+}$ ions (aqueous) are substantially more complex than those for $[Pro_n + H]^{+}$ ions (Figure 4) and indicate the presence of a wide range of conformer types. Here, we focus on comparing the experimental cross section for the most intense peaks observe at each polymer size (given in Figure 5 and Table 1) with theory but note that the conformers shown are only part of a more complicated conformer landscape.

The low-energy PPI-derived geometries described above (Figure 9a) have calculated cross sections that are too large to be considered as representative of the conformations of $[Pro_n + 2H]^{2+}$ (aqueous) ions observed from experiment. Figure 9c presents model representative structures obtained by starting from ideal PPII helices. Four different charge site assignments are shown for $[Pro_{15} + 2H]^{2+}$: (1,2), (1,7), (1,15), and (7,15). The types of structures illustrated are typical of the other lengths examined computationally ($[Pro_{10} + 2H]^{2+}$ and $[Pro_{20} + 2H]^{2+}$). Protonation of two sites at the N-terminal side of the peptide [e.g., the (1,2) conformer] yields structures that are low in energy, but more compact than expected from the experimental distribution (for all three polymer lengths). Protonation of sites at the amino terminus and near the C-terminal end [e.g., (1,15)] yield highly extended conformations that have collision cross sections higher than those derived from the measured distributions. The calculated collision cross section of the (1,7) conformer is in very good agreement with experiment (Ω_{calc} = 326.3 Å^2; Ω_{expt} = 328.7 Å^2). The (7,15) conformer has a

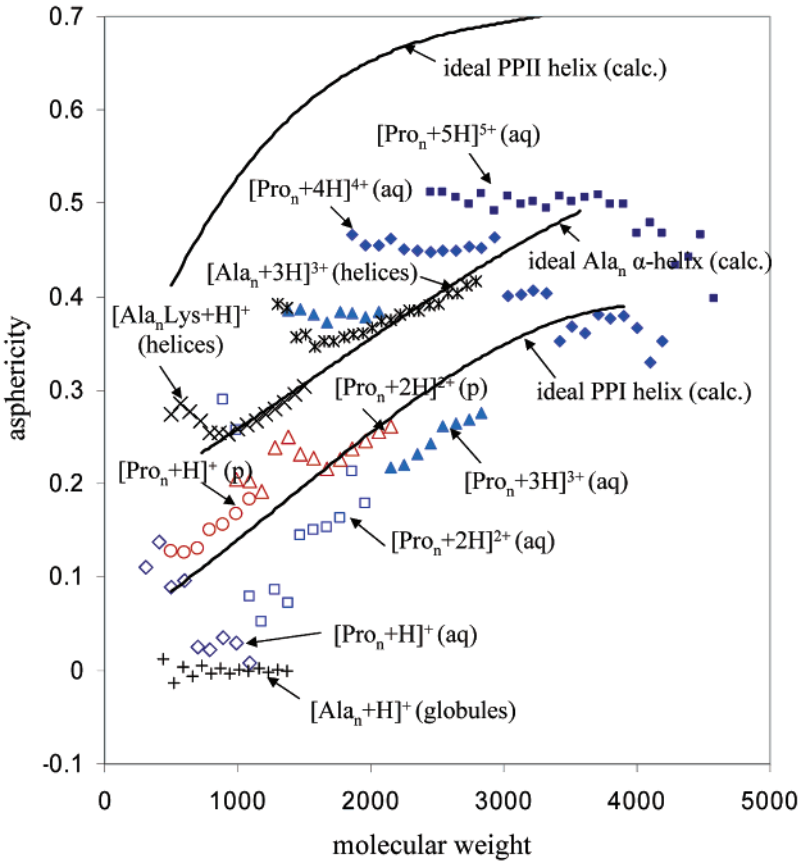

Figure 7. Asphericities for peak maxima observed at each m/z ratio in ion mobility/time-of-flight data sets recorded for $[Pro_n + zH]^{z+}$ ions electrosprayed from 49:49:2 water/methanol/acetic acid solutions: Symbols represent the following: open diamonds, $[Pro_n + H]^+$ ions; open squares, $[Pro_n + 2H]^{2+}$; solid triangles, $[Pro_n + 3H]^{3+}$; solid diamonds, $[Pro_n + 4H]^{4+}$; solid squares, $[Pro_n + 5H]^{5+}$. Asphericities for ions formed by electrospraying from propanol solution are indicated by open circles ($[Pro_n + H]^+$) and open triangles ($[Pro_n + 2H]^{2+}$). Symbols "+", "×", and "*" are used to represent asphericities measured for $[Ala_n + H]^+$ globules, $[Ala_nLys + H]^+$ α-helices, and $[Ala_n + 3H]^{3+}$ extended helices, respectively. The solid lines represent fits (as a function of molecular weight) to calculated cross sections for ideal PPI and PPII helical forms (Figure 1).

collision cross section that is slightly higher than experiment (by 3.7%). In both of these conformers, the polymer is folded in a hairpin-like shape. The position of the bend appears to be linked to the position of the charge site (analogous to our observations of hinged helix-coil conformers in $[Ala_n + 3H]^{3+}$ peptides).[19] We further note that solvation of the charge sites in the polyproline system should be less facile relative to other polyamino acids because of the increased energetic cost associated with rotation around the Pro-Pro peptide bond.

The hairpin structural types may explain the complicated distributions observed in our experiments. Depending on the exact protonation sites of the polymer upon complete desolvation in the electrospray process, the polymer may fold at a different location. It seems probable that there are many low-energy states in which the polymer is folded. At longer polymer sizes, the Coulombic repulsion between charge sites will be reduced in the hairpin-like structure, allowing lower energy states that are more compact to be sampled.

General Characteristics of Larger Polyproline Ions. None of the conformers that we observe from aqueous solution appear to be as extended as the PPII helical form. Upon dehydration during the electrospray process, it appears likely that a mixture of cis- and trans-residue forms become favored in order to increase the van der Waals stabilization and allow hydrogen bonding between charge sites and carbonyl groups on the peptide backbone. This was demonstrated for the relatively compact, roughly globular $[Pro_{10} + H]^+$ ions (Figure 8c) and also seems to be required for more extended conformers. Figure 10 shows molecular dynamics simulations for $[Pro_{15} + 3H]^{3+}$ that support this idea. The conformations shown are the lowest energy structures obtained from simulations started from PPI, PPII, and geometries in which the cis and trans residues were randomized. The geometry obtained from PPI starting structures retains most (but not all) of its cis-residue content but is unraveled, particularly near the termini; the calculated cross section for this structure is slightly lower (2%) than experiment. The conformation derived from a PPII starting geometry is highly extended and has a cross section ~10% higher than experiment. The (1,8,15) conformer started from random cis- and trans-residue orientations is the lowest energy conformer found over all simulations of $[Pro_{15} + 3H]^{3+}$ and is within 0.3% of the experimental cross section. Clearly, we have not sampled all possible proton configurations or randomization of cis and trans residues; there should be many conformers that also provide good agreement with experiment. The salient points to note about this type of structure that agrees with experiment are that it is extended (although not as extended as PPII) and contains a mixture of cis- and trans-residue forms.

In general, within a charge state (for $z \geq 2$), small polymer sizes appear to favor relatively extended conformations with a combination of cis- and trans-residue forms. It seems likely that many different combinations of cis- and trans-residue positions will be present and that a range of these will have cross sections that are consistent with experiment.

It is interesting that these ions favor relatively extended conformations, substantially more open than we have observed

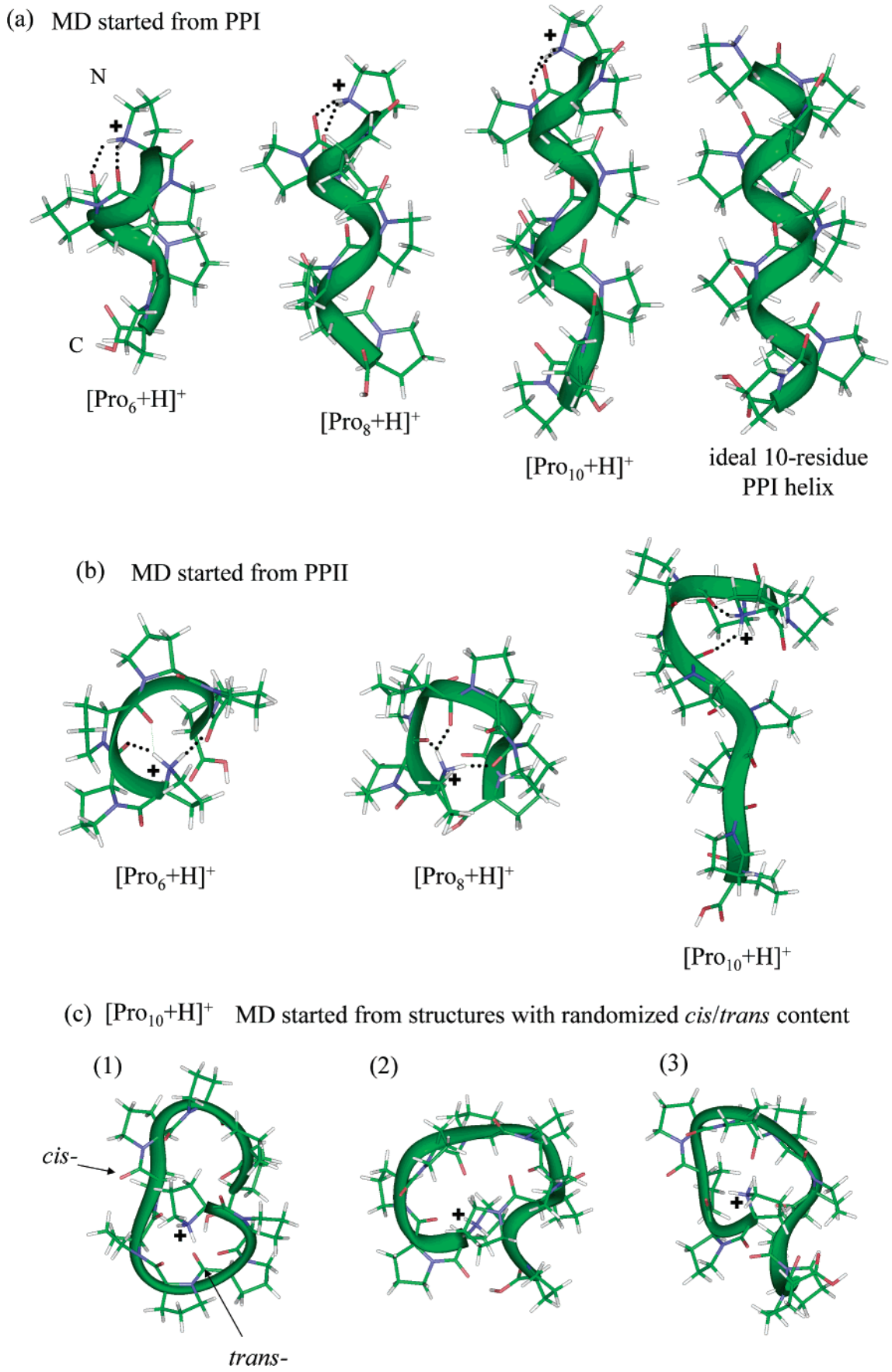

Figure 8. Lowest energy conformers obtained from molecular dynamics simulations of $[Pro_6 + H]^+$, $[Pro_8 + H]^+$, and $[Pro_{10} + H]^+$ started from (a) polyproline I and (b) polyproline II initial structures. An ideal 10-residue PPI helix is included for comparison. Part c shows representative low-energy conformers for $[Pro_{10} + H]^+$ obtained from starting geometries in which the conformations of individual proline residues (cis or trans) along the polymer were randomized. Experimental and calculated cross sections are given in Table 1.

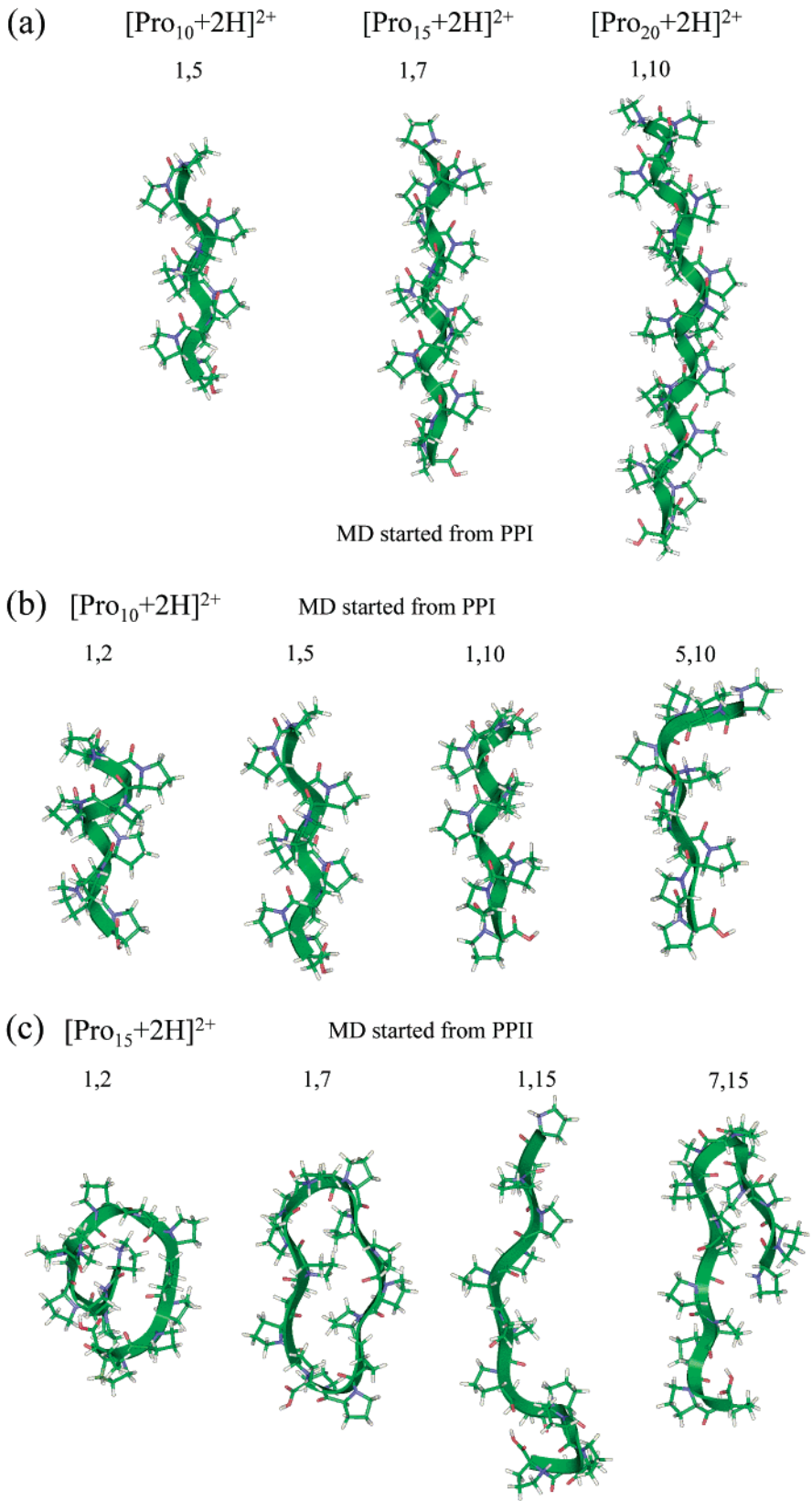

Figure 9. (a) Representative low-energy conformers for $[Pro_{10} + 2H]^{2+}$, $[Pro_{15} + 2H]^{2+}$, and $[Pro_{20} + 2H]^{2+}$ obtained from PPI starting geometries in which the protons were placed on the N-terminus and a backbone imide at the midpoint of the polymer (i.e., *n*/2). (b) Low-energy conformers obtained from simulations of $[Pro_{10} + 2H]^{2+}$ in which protons were located in the (1,2), (1,5), (1,10), and (5,10) positions on a PPI starting geometry. Pairs of numbers indicate position of the protonated imides along the backbone of the peptide (e.g., 1 denotes the N-terminus). (c) Representative low-energy conformations for $[Pro_{15} + 2H]^{2+}$ obtained from a PPII starting geometry for (1,2), (1,7), (1,15), and (7,15). Experimental and calculated cross sections for all conformers shown are given in Table 1.

for other polyamino acids [poly(Xxx), where Xxx = Val, Ile, Leu, Gln, Thr, Phe, and Trp][45] as well as heterogeneous sequences, such as tryptic peptides of similar size.[46] Several factors may aid in favoring extended structures. For example,

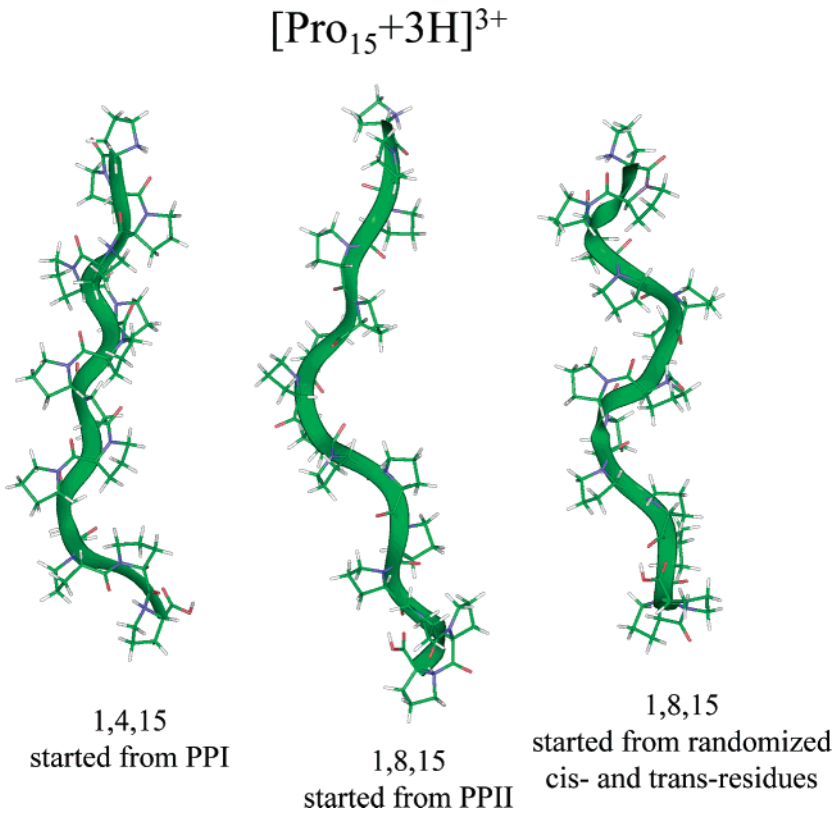

Figure 10. Lowest energy conformers obtained for $[Pro_{15} + 3H]^{3+}$ by started molecular dynamics simulations from a PPI helix, PPII helix, and conformers in which the cis- and trans-residue content was randomized. Numbers indicate protonation sites. The calculated cross sections for these conformers are 386.4 Å^2, 433.0 Å^2, and 393.2 Å^2, respectively. The experimental collision cross section for $[Pro_{15} + 3H]^{3+}$ is 394.0 Å^2.

as reported for other systems, high charge states may adopt extended geometries in order to reduce Coulombic interactions. We note also that polyproline (unlike other polyamino acids and heterogeneous peptide sequences) does not appear to pack efficiently. The difference of polyproline compared with other polyamino acids is that the conformations are much more restricted, based on the constraints imposed by covalent attachment of the five-membered ring at two points along the peptide backbone. Other amino acids display an ability to pack tightly in the gas phase. In fact, average individual amino acid volumes are ~5% to 15% smaller in gas-phase peptides ions than in solution.[46] A common feature of packing in these systems is that side chains pack efficiently into grooves and crevices; the efficiency of this packing appears to be facilitated by slight rearrangements of torsion angles along the peptide backbone. The polyproline system is simply restricted to a much greater degree, and gas-phase stabilization through efficient packing is much less pronounced. Having said this, at larger polymer sizes, some polymer folding is observed. From the limited number of molecular dynamics simulations we have performed on highly charged $[Pro_n + zH]^{z+}$ ions, the ion mobility measurements for the most compact states are not consistent with tightly packed globular structures. The discrete features within the broad distributions that are measured suggest that there may be favored states in the folding pathways of these ions. We cannot rule out the possibility that these peaks are not along the folding coordinate but rather correspond to a number of low-energy or kinetically trapped states.

Summary and Conclusions

Ion mobility/time-of-flight measurements and molecular modeling simulations have been employed to investigate the gas-phase conformations of a series of polyproline ions, $[Pro_n + zH]^{z+}$ ($n = 3-56$; $z = 1-6$), obtained by electrospraying aqueous and propanol solutions. Overall, we find that this system is very complex. We find evidence for multiple structural types that depend on polymer size, charge state, and initial solvent composition. Because of the complexity of this system, this initial study is largely a survey of the system, and a more detailed analysis of the structures will follow.

This said, some structural information involving relatively small polyproline polymers has been obtained by comparing calculated cross sections for trial molecular modeling geometries to experimental values. The $[Pro_n + H]^+$ and $[Pro_n + 2H]^{2+}$ (propanol) ions are most consistent with stretched all-cis PPI helices. These helices appear to be particularly stable, as they are favored in the propanol solution and persist into the gas phase. The gas-phase stability can be rationalized by considering three favorable aspects of the PPI geometry. The polyproline peptide should be protonated at the most basic site, the amino terminus. Protonation of the PPI structure at this site allows favorable hydrogen-bonding interactions to be established between the protonation site and the carbonyls of the second and third proline residues. Molecular modeling studies indicate that the helix stretches slightly from the ideal PPI conformation (which maximizes van der Waals interactions) to accommodate these hydrogen bonds. Additionally, protonation at the amino terminus in the PPI type of structure stabilizes the macrodipole of the helix. We note that this helix macrodipole is oriented in the opposite direction compared with the classical α- and 3_{10}-helices found in other L-amino acids.

The polyproline (aqueous) system is extremely complex. The highly extended all-trans PPII structure is expected in solution; in vacuo, none of the conformations we observe are as extended as the ideal PPII helix. We interpret the dearth of any evidence for the PPII structure in the gas phase by considering the earlier

solution-phase work.[5,6] Critically important to the stability and solubility of the PPII helix in aqueous solutions is the formation of hydrogen bonds between −OH groups of the solvent and polar backbone carbonyl residues along the polymer. Presumably as the solvent is removed during the electrospray process, the loss of water destabilizes the PPII helix.

Having said this, it is clear why no PPII helix is observed in the gas phase. What is less clear is what these ions look like in the gas phase. The ion mobility/time-of-flight data show distinct peaks that appear to fall into structural families according to polymer size and charge state. The existence of a series of related peaks indicates that preferred structures exist. Comparisons with earlier results for other polyamino acids such as polyXxx (Xxx = Ala, Val, Ile, Leu, Gln, Thr, Phe, and Trp)[20,45] as well as with small proteins[29] indicates that polyproline ions do not pack as efficiently as these polymers. This difference can be rationalized by considering the additional restrictions imposed upon conformations by the covalent attachment of the five-membered ring that comprises the proline side chain as a part of the polymer backbone.

The work described above has considered the structures of small ions formed from aqueous solutions in detail. Comparison of experimental collision cross sections with calculated cross sections from model geometries indicates that the $[Pro_n + H]^+$ ions ($n = 6-11$) can form relatively compact structures; these compact geometries appear to arise from the stability gained by solvating the protonation site through interactions with the peptide backbone. However, $[Pro_n + zH]^{z+}$ ($n > 10$, $z > 1$) from aqueous solutions favor geometries that are not as tightly packed as other polyamino acids. This can be observed by examining the plot of effective asphericities (Figure 7).

The $[Pro_n + 2H]^{2+}$ ions formed by electrospraying aqueous solutions appear to favor structures that are folded, and in some cases we observe hairpin-like geometries. In both cases, a mixture of *cis*- and *trans*-proline forms are required in the initial molecular modeling studies to form structures that have cross sections that are consistent with experiment. Several conformer families are observed for higher charge states in the aqueous system. More compact conformer families arise as polymer size increases within a given charge state (as would be expected upon reduction of Coulombic repulsion). The most compact families observed for $z = 2-4$ appear to form a superfamily of related conformers that are more compact than an ideal PPI helix and less tightly packed than a globule. We speculate that these ions may form hinged structures or perhaps a more compact helical form that is not observed in solution. Molecular dynamics simulations to explore these types of structures are ongoing.

Acknowledgment. Financial support is provided by the National Science Foundation (Grant No. CHE-0078737). We also gratefully acknowledge stimulating discussions with Professors Gary Glish (University of North Carolina) and Martin Jarrold (Indiana University) that led to us initiating these studies.

References and Notes

(1) *Poly-α-amino Acids*; Fasman, G. D., Ed.; M. Dekker; New York, 1967.

(2) IUPAC-IUB Commission on Biochemical Nomenclature. *Biochemistry* **1970**, *9*, 3471.

(3) Kim, H. D. *Bull. Korean Chem. Soc.* **1997**, *18*, 922.

(4) Zheng, N. J.; Rau, G.; Hazlewood, C. F.; Rau, C. *Scanning Microsc.* **1991**, *5*, 631; Rau, C.; Zheng, N. J.; Hazlewood, C.; Rau, G. *Physiol. Chem. Phys. Med. NMR* **1995**, *27*, 55.

(5) Bella, J.; Brodsky, B.; Berman, H. M. *Structure* **1995**, *3*, 893.

(6) Stanley, J. A.; Peemoeller, H. *J. Phys. II* **1991**, *1*, 1491.

(7) Dukor, R. K.; Keiderling, T. A. *Biospectroscopy* **1996**, *2*, 83.

(8) Fenn, J. B.; Mann, M.; Meng, C. K.; Wong, S. F.; Whitehouse, C. M. *Science* **1989**, *246*, 64.

(9) Martin, S. A.; Biemann, K. *Int. J. Mass Spectrom. Ion Processes* **1987**, *78*, 213.

(10) Hunt, D. F.; Yates, J. R.; Shabanowitz, J.; Winston, S.; Hauer, C. R. *Proc. Natl. Acad. Sci. U.S.A.* **1988**, *83*, 6233.

(11) Loo, J. A.; Edmonds, C. G.; Smith, R. D. *Anal. Chem.* **1993**, *65*, 425.

(12) He, M.; Reid, G. E.; Shang, H.; Lee, G. U.; McLuckey, S. A. *Anal. Chem.* **2002**, *74*, 4653.

(13) Breci, L. A.; Tabb, D. L.; Yates, J. R., III; Wysocki, V. H. *Anal. Chem.* **2003**, *75*, 1963.

(14) Counterman, A. E.; Clemmer, D. E. *Anal. Chem.* **2002**, *74*, 1946.

(15) Hudgins, R. R.; Ratner, M. A.; Jarrold, M. F. *J. Am. Chem. Soc.* **1998**, *120*, 12974.

(16) Kinnear, B. S.; Kaleta, D. T.; Kohtani, M.; Hudgins, R. R.; Jarrold, M. F. *J. Am. Chem. Soc.* **2000**, *122*, 9243.

(17) Kaleta, D. T.; Jarrold, M. F. *J. Phys. Chem. B* **2001**, *105*, 4436.

(18) Kinnear, B. S.; Hartings, M. R.; Jarrold, M. F. *J. Am. Chem. Soc.* **2001**, *123*, 5660.

(19) Kinnear, B. S.; Hartings, M. R.; Jarrold, M. F. *J. Am. Chem. Soc.* **2002**, *124*, 4422.

(20) Counterman, A. E.; Clemmer, D. E. *J. Am. Chem. Soc.* **2001**, *123*, 1490.

(21) Srebalus-Barnes, C. A.; Clemmer, D. E. *J. Phys. Chem. A* **2003**, *107*, 10566.

(22) Kinnear, B. S.; Jarrold, M. F. *J. Am. Chem. Soc.* **2001**, *123*, 7907.

(23) Counterman, A. E.; Clemmer, D. E. *J. Phys. Chem. B* **2002**, *106*, 12045.

(24) For recent reviews, see: (a) Clemmer, D. E.; Jarrold, M. F. *J. Mass Spectrom.* **1997**, *32*, 577. (b) Hoaglund Hyzer, C. S.; Counterman, A. E.; Clemmer, D. E. *Chem. Rev.* **1999**, *99*, 3037.

(25) (a) Hoaglund, C. S.; Valentine, S. J.; Sporleder, C. R.; Reilly, J. P.; Clemmer, D. E. *Anal. Chem.* **1998**, *70*, 2236. (b) Henderson, S. C.; Valentine, S. J.; Counterman, A. E.; Clemmer, D. E. *Anal. Chem.* **1999**, *71*, 291.

(26) Li, J.; Taraszka, J. A.; Counterman, A. E.; Clemmer, D. E. *Int. J. Mass Spectrom.* **1999**, *185/186/187*, 37.

(27) Hudgins, R. R.; Woenckhaus, J.; Jarrold, M. F. *Int. J. Mass Spectrom.* **1997**, *165/166*, 497.

(28) (a) von Helden, G.; Wyttenbach, T.; Bowers, M. T. *Science*, **1995**, *267*, 1483. (b) Wyttenbach, T.; von Helden, G.; Bowers, M. T. *J. Am. Chem. Soc.* **1996**, *118*, 8355.

(29) Clemmer, D. E.; Hudgins, R. R.; Jarrold, M. F. *J. Am. Chem.* Soc. **1995**, *117*, 10141.

(30) Valentine, S. J.; Counterman, A. E.; Hoaglund, C. S.; Reilly, J. P.; Clemmer, D. E. *J. Am. Soc. Mass Spectrom.* **1998**, *9*, 1213.

(31) Wu, C.; Siems, W. F.; Asbury, G. R.; Hill, H. H. *Anal. Chem.* **1998**, *70*, 4929.

(32) von Helden, G.; Hsu, M.-T.; Kemper, P. R.; Bowers, M. T. *J. Chem. Phys.* **1991**, *95*, 3835.

(33) Jarrold, M. F.; Constant, V. A. *Phys. Rev. Lett.* **1991**, *67*, 2994.

(34) For recent reviews of ion mobility studies of biomolecules see: (a) Clemmer, D. E.; Jarrold, M. F. *J. Mass Spectrom.* **1997**, *32*, 577. (b) Hoaglund Hyzer, C. S.; Counterman, A. E.; Clemmer, D. E. *Chem. Rev.* **1999**, *99*, 3037.

(35) Effective asphericities are calculated using $\Omega_{sphere} = -9.49 \times 10^{-4}n^3 + -0.213n^2 + 16.2n + 38.1$, as determined from a fit to experimental cross sections for globular $[Ala_n + H]^+$ ions and $\Omega_{linear} = 25.95n + 27.75$, as determined from a fit to calculated cross sections (as described in ref 19) for linear structures.

(36) Ewing, N. P.; Zhang, X.; Cassady, C. J. *J. Mass Spectrom.* **1996**, *31*, 1345.

(37) Because of limitations in our modeling software, we chose to place protons on imide nitrogens of the proline residues rather than at the more basic carbonyl oxygens [for measurements of proton affinities, see, for instance, the following: (a) Zhang, K.; Cassady, C. J.; Chung-Phillips, A. *J. Am. Chem. Soc.* **1994**, *116*, 11512. (b) Addario, V.; Guo, Y.; Chu, I. K.; Ling, Y.; Ruggerio, G.; Rodriguez, C. F.; Hopkinson, A. C.; Siu, K. W. M. *Int. J. Mass Spectrom.* **2002**, *219*, 101]. Our justification for placing the protons is that for these large systems, Coulombic repulsion between charges is the dominant driving force (as observed in our work on large, multiply protonated polyalanine systems; see, for instance, refs 20 and 23). Our measurement allows us to discriminate between different conformer types (such as different types of helices or globules) but does not provide the ability to resolve structures at atomic resolution. In modeling the large polymer systems examined here, the exact placement of protonation sites should not significantly affect the results.

(38) Drakenberg, T.; Forsen, S. *J. Phys. Chem.* **1970**, *74*, 1.

(39) Roques, B. P.; Garbay-Jaureguiberry, C.; Combrisson, S.; Oberlin, R. *Biopolymers* **1977**, *16*, 937.

(40) Cheng, H. N.; Bovey, F. A. *Biopolymers* **1977**, *16*, 1465.

(41) Albers, M. W.; Walsh, C. T.; Schruber, S. L. *J. Org. Chem.* **1990**, *55*, 4984.
(42) Shvartsburg, A. A.; Jarrold, M. F. *Chem. Phys. Lett.* **1996**, *261*, 86.
(43) Mesleh, M. F.; Hunter, J. M.; Shvartsburg, A. A.; Schatz, G. C.; Jarrold, M. F. *J. Phys. Chem.* **1996**, *100*, 16082.
(44) Calculated m/z values (m/z_{calc}) are computed for each polymer size (n) and charge state (z) using a Pro residue mass of 97.1; that is, $m/z_{calc} = (97.1n + z)/z$.
(45) Henderson, S. C.; Li, J.; Counterman, A. E.; Clemmer, D. E. *J. Phys. Chem. B* **1999**, *103*, 8780.
(46) Counterman, A. E.; Clemmer, D. E. *J. Am. Chem. Soc.* **1999**, *121*, 4031.